Extended Data Fig. 1. The cytotoxicity of H84T-BanLec in different cell lines. The cytotoxicity of H84T-BanLec in VeroE6, Huh7, BSC-1, HELF, and Calu-3 cells was evaluated using the CellTiterGlo® luminescent cell viability assay according to manufacturer's instructions. H84T-BanLec did not display any obvious cytotoxicity in any of these cell lines even at the concentration of 10μM (ie: 10,000nM).

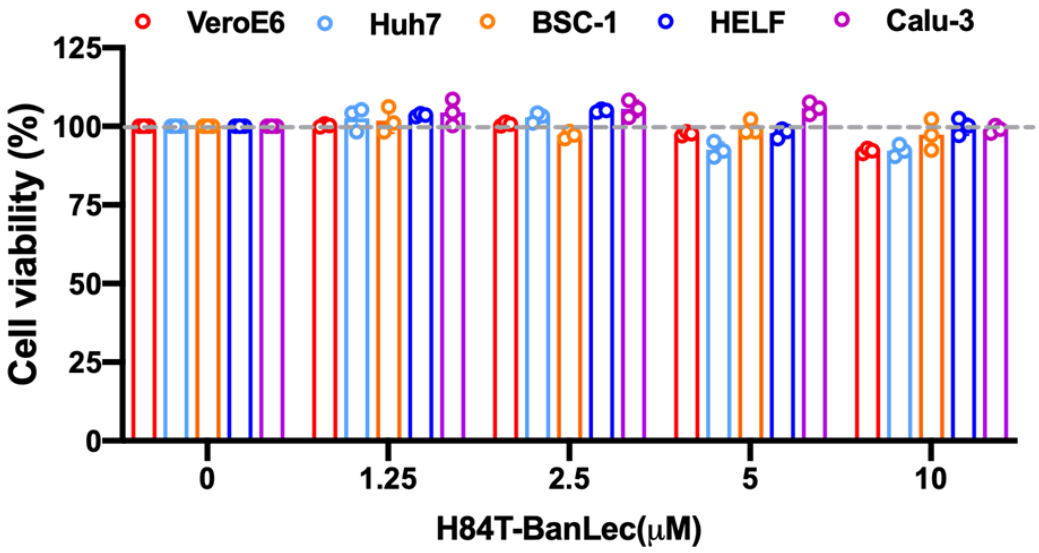

Extended Data Fig. 2. Antiviral activity of H84T-BanLec against other human-pathogenic coronaviruses. The antiviral activity of H84T-BanLec against SARS-CoV by **a,** plaque reduction assay and **b, (left)** viral load reduction assay; and **b, (right)** against HCoV-229E by viral load reduction assay.

(a)

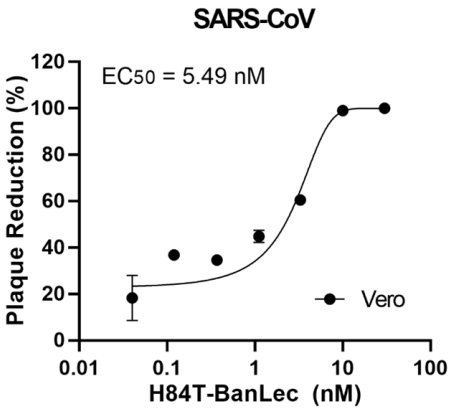

(b)

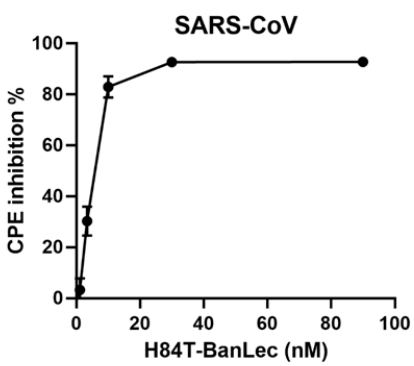

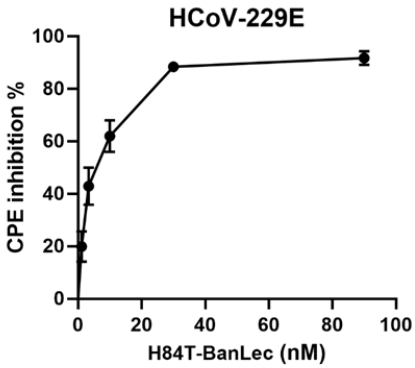

Extended Data Fig. 3. Antiviral activity of H84T-BanLec against emerging SARS-CoV-2 variants. The antiviral activity of H84T-BanLec against SARS-CoV-2 **a,** B.1.1.7 (with N501Y) and **b,** P.3 (with N501Y, E484K, and 141 to 143 deletion) variants were evaluated by **(left)** viral load reduction and **(right)** plaque reduction assays in VeroE6 cells. Data are mean ± s.d., n = 3 biological replicates. One-way ANOVA. ***P<0.001, **P<0.01, *P<0.05.

(a)

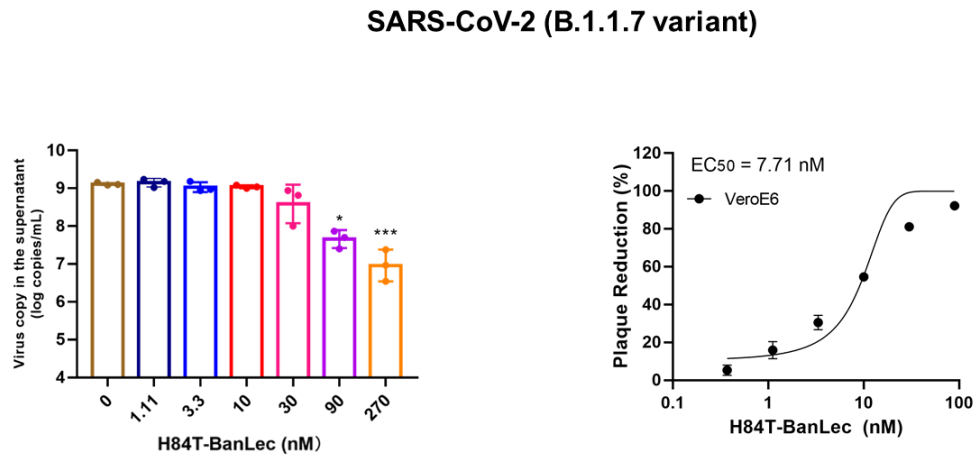

(b)

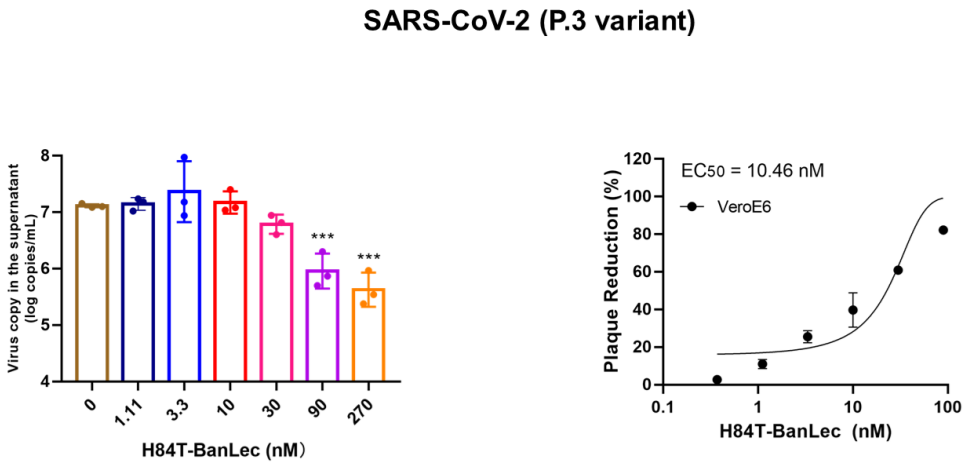

Extended Data Fig. 4. H84T-BanLec targets virus internalization during coronavirus entry. a, Time-of-drug-addition assay indicated that H84T-BanLec interfered with SARS-CoV-2 entry. **b,** Virus attachment and **c,** virus internalization assays showed that H84T-BanLec targeted the internalization rather than attachment to inhibit SARS-CoV-2 replication. Student's t-test. ***P*<0.01.

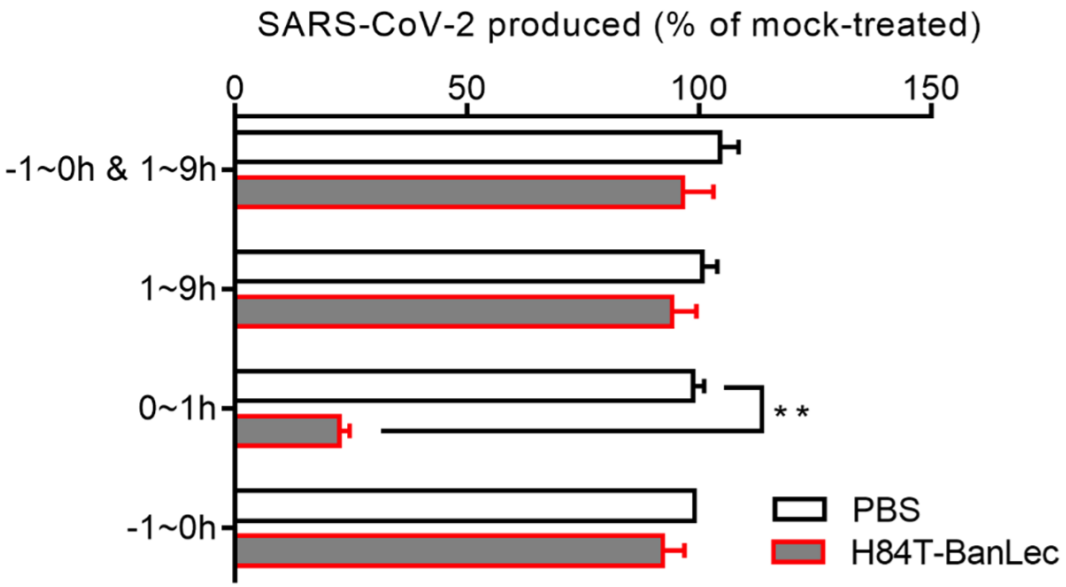

Extended Data Fig. 5. Co-localization of H84T-BanLec with SARS-CoV-2 spike protein in the autopsied lung section of a deceased COVID-19 patient. Top, Multiplex immunohistochemical analysis of SARS-CoV-2-infected autopsy lung section (SARS-CoV-2 nucleocapsid protein, yellow; SARS-CoV-2 spike protein, red; and H84T-BanLec, orange). Total original magnification 200×. Sections were counterstained with DAPI to visualize nuclei (blue) and scanned using the Polaris Vectra multiplex spectral scanner. **Bottom,** The digital metadata were uploaded to FIJI for co-localization. The mean pixel intensity for each fluorochrome (0-256) at a particular centroid was plotted and the number of co-localizations calculated. The Pearson correlation calculation ranged from -1 to +1 and indicated inverse correlation (-1) through no correlation (0) to positive correlation (+1). The values calculated (0.6 and 0.58) for spike protein vs nucleocapsid protein and spike protein versus H84T-BanLec respectively represented high degrees of co-localization.

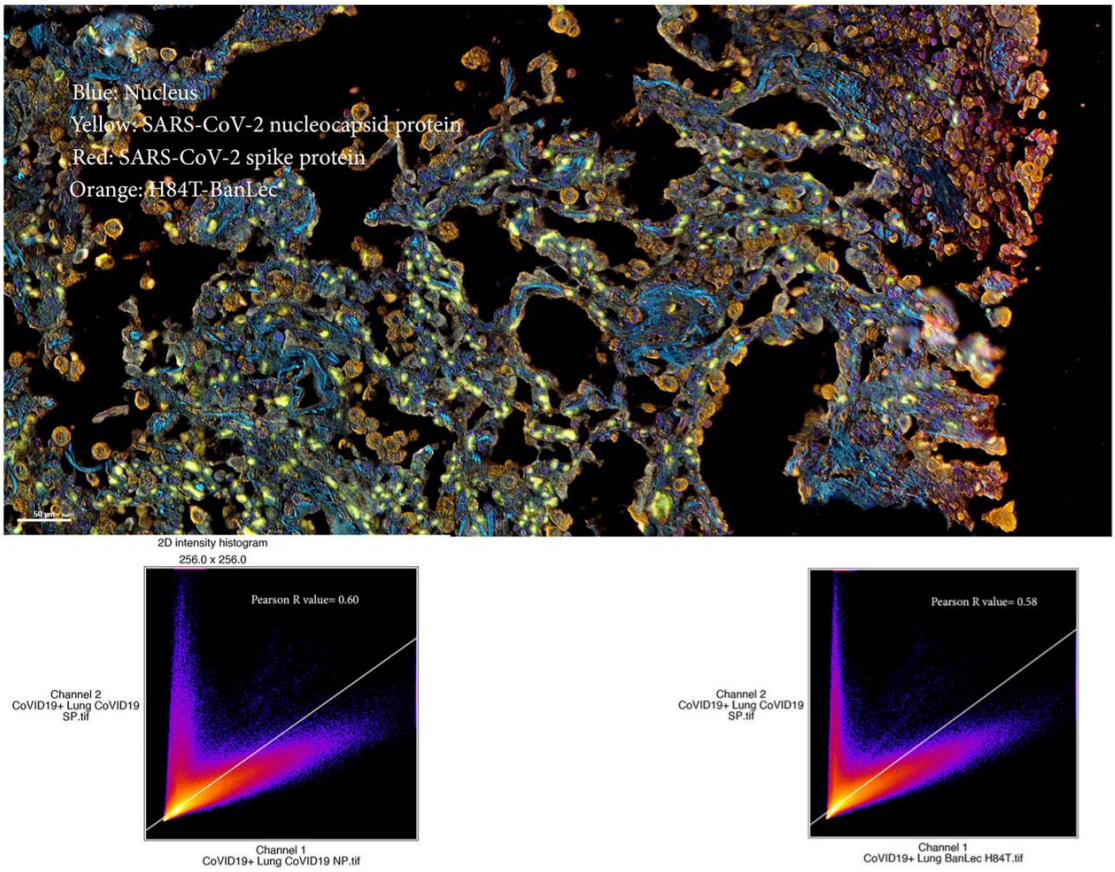

Extended Data Fig. 6. Surface plasmon resonance (SPR) measurements. H84T-BanLec was injected at the indicated concentrations to surfaces containing immobilized **a,** full-length trimeric N234Q spike mutant or **b,** receptor-binding domain to allow for binding (ascending parts), followed by wash out using buffer (descending parts). Data were fitted using the bivalent binding model, consistent with H84T-BanLec being predominantly a dimer.

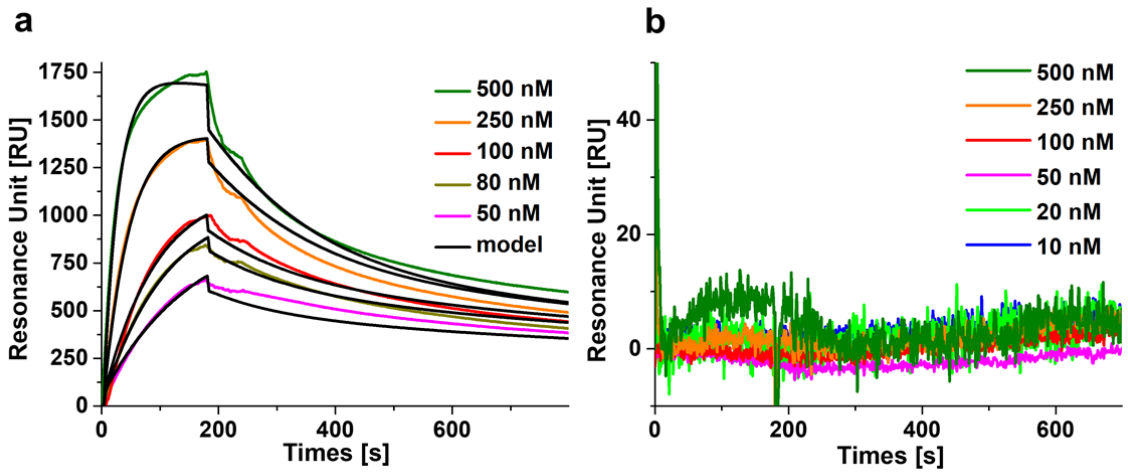

Extended Data Fig. 7. Binding activity of SARS-CoV-2 spike protein to H84T-BanLec. SARS-CoV-2 spike protein coupled to an AFM cantilever tip to the surface of VeroE6 cells in the presence of H84T-BanLec probed at the indicated concentrations in solution during single molecule force spectroscopy experiments. Measurements were done on at least 5 cells and at minimum 100 force-distance cycles were recorded on each cell at the respective H84T-BanLec concentrations. The binding activity was calculated from the fraction of force curves showing unbinding events. H84T-BanLec effectively blocks binding of SARS-CoV-2 spike protein to VeroE6 cells at 10nM concentration.

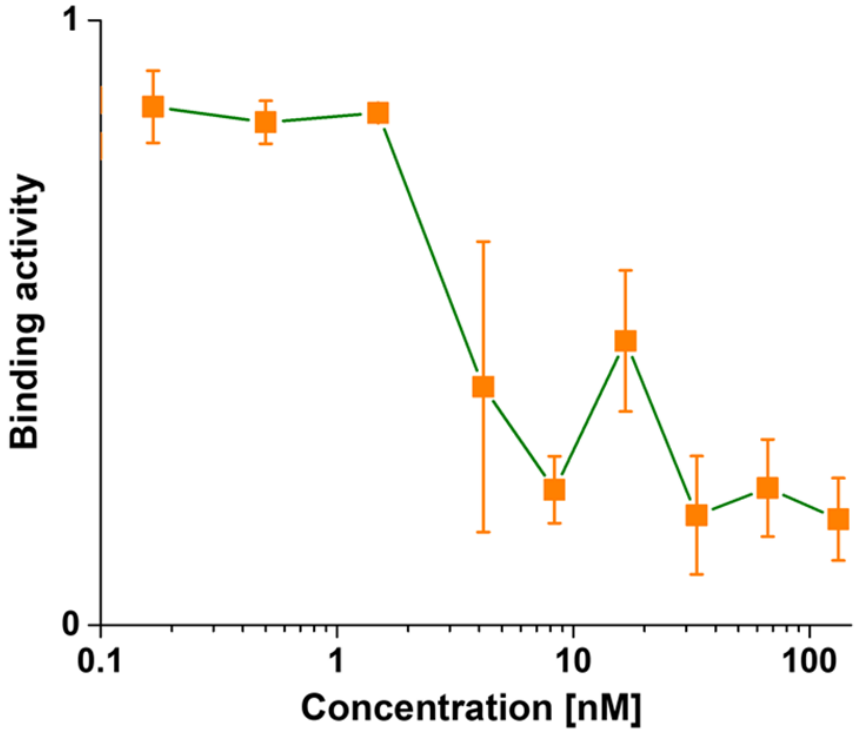

Supplementary Table S1. Quantification of parameters obtained with dynamic force spectroscopy (DFS) and surface plasmon resonance (SPR) methods. k_{on}, k_{off}, and K_D, are kinetic on-rate, kinetic off-rate, and equilibrium dissociation constant, respectively, of a single bond (DFS) or the first binding step (SPR). X_β denotes the distance of the activation barrier from the energy minimum along the pulling axis in DFS experiments.

	Dynamic Force Spectroscopy (DFS)	**Surface Plasmon Resonance (SPR)**	
	H84T-BanLec/Spike trimer	H84T-BanLec/Spike trimer	H84T-BanLec/N234Q spike mutant
$k_{off,\,1}$ **[1/s]**	0.0457 ± 0.024	0.0262 ± 0.007	0.006 ± 0.0027
$k_{on,\,1}$ **[1/Ms]**	$9.98 \times 10^{4} \pm 5.18 \times 10^{4}$	$2.09 \times 10^{4} \pm 0.25 \times 10^{4}$	$2.99 \times 10^{4} \pm 0.31 \times 10^{4}$
K_D **[M]**	$4.60 \times 10^{-7} \pm 4.37 \times 10^{-7}$	$1.28 \times 10^{-6} \pm 0.19 \times 10^{-6}$	$2.17 \times 10^{-7} \pm 1.14 \times 10^{-7}$
X_β **[Å]**	7.825 ± 0.603		

Supplementary Video S1. The dynamics of the H84T-BanLec/SARS-CoV-2 spike protein interactions filmed with real-time high-speed AFM under physiological conditions. The video was recorded at a scan speed of 303 ms/frame. Scan size 100 × 100 nm^2.